Femtomolar detection by nanocoated fibre label-free biosensors

Francesco Chiavaioli,[1,‡,*] Pablo Zubiate,[2,‡] Ignacio Del Villar,[3,*] Carlos R. Zamarreño,[2] Ambra Giannetti,[1] Sara Tombelli,[1] Cosimo Trono,[1] Francisco J. Arregui,[3] Ignacio R. Matias,[3] Francesco Baldini[1]

1 Institute of Applied Physics "Nello Carrara" (IFAC), National Research Council of Italy, 50019 Sesto Fiorentino, Firenze, Italy. 2 Electrical and Electronic Engineering Department, Public University of Navarra, 31006 Pamplona, Spain. 3 Institute of Smart Cities (ISC), Public University of Navarra, 31006 Pamplona, Spain.

Keywords: *Optical biosensor, lossy mode resonance, optical fibre sensor, nanometric metal oxide film, label-free biomolecular interaction, femtomolar detection limit, regeneration*

ABSTRACT: The advent of optical fibre-based biosensors combined with that of nanotechnologies has provided an opportunity for developing *in situ*, portable, lightweight, versatile and high-performance optical sensing platforms. We report on the generation of lossy mode resonances by the deposition of nm-thick metal oxide films on optical fibres, which makes it possible to measure precisely and accurately the changes in optical properties of the fibre-surrounding medium with very high sensitivity compared to other technology platforms, such as long period gratings or surface plasmon resonances, the gold standard in label-free and real-time biomolecular interaction analysis. This property, combined with the application of specialty structures such as D-shaped fibres, permits enhancing the light-matter interaction. SEM and TEM imaging together with X-EDS tool have been utilised to characterise the two films used, i.e. indium tin oxide and tin dioxide. Moreover, the experimental transmission spectra obtained after the deposition of the nanocoatings have been numerically corroborated by means of wave propagation methods. With the use of a conventional wavelength interrogation system and ad-hoc developed microfluidics, the shift of the lossy mode resonance can be reliably recorded in response to very low analyte concentrations. Repeated experiments confirm a big leap in performance thanks to the capability to detect femtomolar concentrations in human serum, improving the detection limit by three orders of magnitude when compared with other fibre-based configurations. The biosensor has been regenerated several times by injecting sodium dodecyl sulphate, which proves the capability of sensor to be reused.

Over recent decades, optical fibre sensors (OFSs) have progressively gained a higher market share, while research on this topic continues to increase.[1] This success has been mainly due to the intrinsic properties of optical fibres (small size, immunity to electromagnetic and radiofrequency interferences, capability to be used in harsh environments and within multiplexed sensing schemes), which make it possible to design compact and lightweight high-performance devices. Recently, the possibility of depositing nano-coatings on optical fibres with a high degree of accuracy and reproducibility has enabled a widening of the domains of application of this technology.[2–4] OFSs are usually reserved for niche applications, such as structural health monitoring,[5] gyroscopes,[6] etc. However, in the recent years, since the community of life sciences and biomedicine is increasingly requesting effective diagnostic and analytical methods capable of detecting target biomolecules at ultra-low limits of detection (LOD), down to pM,[7–10] this gives the possibility of opening the market for early diagnosis of diseases to OFSs.

One of the most well-known phenomena related to thin films for sensing purposes is surface plasmon resonance (SPR),[11,12] even if it is not the only one. In optical sensing, on the basis of some studies carried out using semiconductor waveguides, the concept of guided mode resonance[13] has also been applied to thin film coated OFSs,[14,15] under the name of lossy mode resonance (LMR). Because of the demand for the generation of this kind of resonance, nanocoating must have a complex refractive index (RI) that gives rise to lossy modes.[16,17] In this case, the transmission spectrum of an LMR-based sensor will be characterized by one (first LMR) or more LMR bands in a well-defined wavelength range.[17]

LMRs occur when the real part of the thin film permittivity is positive and greater in magnitude than both its own imaginary part and the permittivity of the material surrounding the thin film.[13] That is why metallic oxides[15,18] and polymers[19] are used to lead to the generation of LMRs, instead of the metallic materials, typically used for obtaining SPRs[3,20] for which the condition for resonance generation is that the real part of the thin film permittivity be negative and greater in magnitude than both its own imaginary part and the permittivity of the material surrounding the thin film. Differently from SPRs, LMRs can be excited both with TE- and TM-polarized light. Thanks to the cylindrical symmetry of the optical fibres, it is possible to observe the resonance that corresponds to each of these polarizations if the real part of the nanocoating RI is high, because the central wavelength of each resonance is quite different.[17] Otherwise, only a single resonance can apparently be appreciated in the transmission spectrum, one

that is a combination of the spectrally close-located TE and TM LMRs.[21]

Another interesting property is that multiple resonances can be attained in the same spectrum,[19] and this makes it possible to monitor a specific parameter at different wavelengths and to reduce the detection error. However, the most important advantage is the possibility of tuning the position of the LMR very easily by controlling the thickness of the nanocoating deposited.[17] Reference[21] provides some rules for the design and the optimization of sensitivity in LMR-based sensors, which can be basically summarised by two main points. First, the adequate selection of a high RI material for the fabrication of the nanocoating enables to increase the sensitivity. Second, the accurate adjustment of the thickness of the nanocoating allows monitoring the LMR in the wavelength range of the detector.

The reduction in the LMR spectral width is another important element. In this sense, the figure of merit (FOM), defined as the ratio between the sensitivity and the full width at half maximum of a resonance,[22] is a key parameter that makes it possible to indicate the quality of a sensor. The application of thin films to D-shaped single-mode fibres (SMFs) has enabled a significant improvement in the FOM as compared to unclad multimode fibres (MMFs), when the bulk RI of the surrounding medium is measured.[17] This is possible because the asymmetric shape of the transversal section of this fibre permits a separation of the TE and TM contributions by using a standard single-mode fibre combined with a polarizer.[14,23] In unclad MMFs, the LMR is due to losses in each mode guided through the optical fibre when one of the modes exhibits a transition to guidance in the nanocoating. Conversely, in D-shaped SMFs, the LMR is caused by losses in the mode guided through the core.[17] This is why a narrow resonance is obtained, which makes it possible to track wavelength shifts with the first LMR, the most sensitive LMR, at wavelengths in the infrared, where the sensitivity is also enhanced if compared to the visible region.[2] This is not possible with nanocoated unclad MMFs, which generate broad resonances that are difficult to analyse. For this type of device, it is necessary to track the second resonance in the visible region, which leads to a reduced sensitivity.[21]

This technology can have a large impact on biosensing, in which the requirement of very low LODs is high in many applications and for which the use of optical fibre has been emerging as a powerful technology.[24] The sensing principle is quite simple: when a target analyte interacts with the thin film coated surface on which a biological sensing layer is deposited, a change in the optical properties of the coating (effective RI) is induced due to surface RI changes and a change in the LMR takes place. These can be measured accurately and precisely by means of an optical transmission setup. It is worth noticing that the results achieved with changes in the bulk RI cannot be automatically transferred to the case of RI changes limited to the thickness of the biological sensing layer.[2]

In this work, we analyse the biosensing performances with an IgG/anti-IgG assay carried out with an IgG sensing layer deposited on the surface of different fibres. First, we characterise unclad MMFs coated with two different nanocoatings: indium tin oxide (ITO) and tin dioxide (SnO_2). Then, the best performing nanocoating is applied to D-shaped SMFs. The results show that it is possible to obtain femtomolar LODs with D-shaped SMFs, a value never attained with optical fibre-based biosensors, which improves the best value obtained with unclad MMFs by three orders of magnitude.

Experimental Section

Materials.

Two different materials for the target were used, i.e. ITO and SnO_2, both with a 99.99% of purity, and they were purchased from ZhongNuo Advanced Material Technology Co. The methacrylic acid/methacrylate copolymer (Eudragit L100) was purchased from Evonik Degussa GmbH (Düsseldorf, Germany). Mouse IgG and goat anti-mouse-IgG were purchased from Zymed Laboratories, Invitrogen Immunodetection (Milan, Italy). 1-Ethyl-3-(3-dimethylaminopropyl) carbodiimide hydrochloride (EDC) and N-hydroxysuccinimide (NHS) were purchased from Pierce (Illinois, USA). Human serum (C Reactive Protein Free Serum) was purchased from HyTest Ltd. (Turku, Finland). All the other reagents, unless otherwise stated, were purchased from Sigma-Aldrich (Milan, Italy).

Fabrication of ITO and SnO_2 thin film coated fibres.

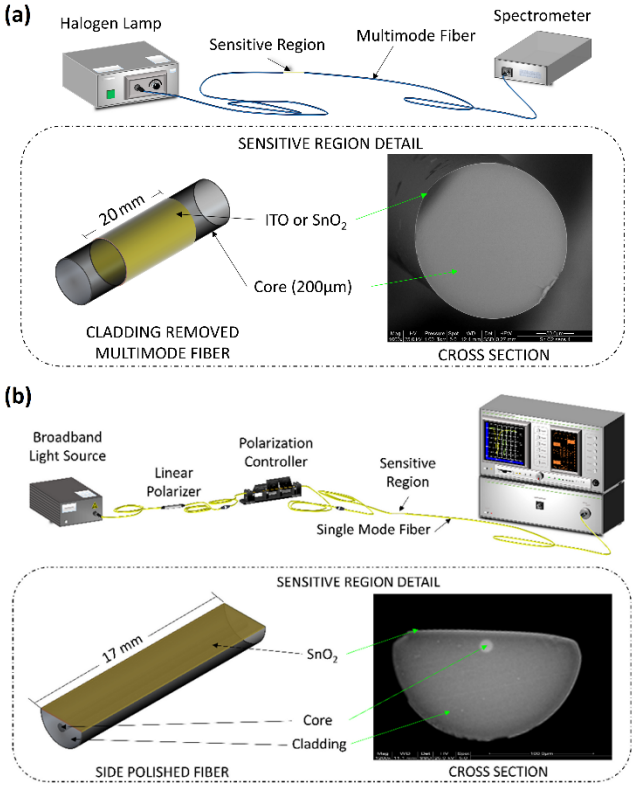

Figure 1. (a) The experimental setup for unclad MMF samples composing of a halogen lamp, a spectrometer and a 20 mm-long sensitive region realized with a thin film of ITO or SnO_2 deposited. (b) The experimental setup for D-shaped SMF samples composing of a multi-LED source, an in-line polarizer, a polarization controller, which permits to excite the D-shaped SMFs with a TE or a TM polarized signal, an optical spectrum

analyser, which monitors the optical spectra, and a 17 mm-long side-polished sensitive region with a thin film of SnO_2 deposited.

Two different types of optical fibres were nanocoated: plastic-clad multimode silica fibres of 200/225 µm core/cladding diameter (FT200EMT) from Thorlabs Inc. and D-shaped single-mode fibres from Phoenix Photonics. The cladding of the FT200EMT fibres was removed in a portion of 20 mm in order to deposit the thin film (see Figure 1a). The unclad MMFs were cleaned as described in reference[25] and then coated with a thin film. The D-shaped SMFs consisted of a standard single mode fibre Corning® SMF-28 with a side-polished length of 17 mm (see Figure 1b). The polished surface of the optical fibres, henceforth called sensitive region, was then coated with a thin film.

Regarding the coating procedure of the thin film deposition, both the unclad MMFs and the D-shaped SMFs were placed on the substrate in a DC sputter machine (ND-SCS200 from Nadetech S.L.). The parameters used in the experiment were partial pressure of argon 9×10^{-2} mbar and intensity 150 mA for ITO target and partial pressure of argon 9×10^{-2} mbar and intensity 90 mA for SnO_2 target. The size of both sputtering targets were 57 mm in diameter and 3 mm in thickness.

Transmission spectrum measurements.

In order to monitor the optical spectrum during the deposition of the thin film and the biosensor experiment, two setups were used. For the unclad MMFs, the experimental setup depicted in Figure 1a was utilised. A halogen lamp (Carl Zeiss CLH 500), which covered a band of 380 to 1140 nm, was connected to one end of the optical fibre. The other end was connected to a spectrometer (Hamamatsu MiniSpectrometer TG-SWNIR C9405CA) that made it possible to monitor the wavelength range from 432 nm to 1145 nm. The experimental setup for the D-shaped SMFs is depicted in Figure 1b. Light from a broadband multi-LED light source (FIBRELABS, Inc., SLD-1310/1430/1550/1690) was transmitted through a thin film coated D-shaped SMF. The output of the fibre was connected to an optical spectrum analyser (OSA, Anritsu MS9030A-MS9701B) that made it possible to monitor a wavelength range from 1200 to 1700 nm. A fibre optic in-line polarizer and a polarization controller, which permits to excite the D-shaped SMFs with a TE or a TM polarized signal, were enclosed between the broadband source and the fibre.

Fibre functionalization and bioassay protocol.

The functionalization of the sensitive portion of both the fibre types was obtained by means of poly(methyl-methacrylate) polymeric (Eudragit L100) deposition, which provided carboxylic functional groups (-COOH), necessary for antibody immobilization, on the surface. The fibre was immersed in 2 mM (0.04% w/v) Eudragit L100 in ethanol for 1 minute, and was then left to dry in the air for about 15 minutes until the solvent had completely evaporated. The fibre was subsequently placed inside an ad-hoc developed thermo-stabilised flow-cell, which allowed keeping the temperature constant at 22°C (±0.05 °C), and glued with an UV-polymerising optical adhesive (NOA 68, Norland Products Inc.). For the sake of clarity, all the next steps of the bioassay protocol are detailed in Supporting Information.

After the bioassay had been completed, a regeneration step was performed in order to regenerate the surface, thus leaving the biological sensing layer intact. A 1% (w/v) sodium dodecyl sulphate (SDS) solution in PBS was used for 3 minutes (flow rate of 25 µL min^{-1}). Afterwards, a rinsing step in PBS was performed before recording the signal baseline.

SEM and TEM imaging.

A transmission electron microscopy (TEM), model TEM CM 12 PHILIPS, equipped with an OLYMPUS Megaview G2 camera that had an accelerating voltage of 80 keV was used to carry out thickness measurements on the fibre samples. Samples for TEM analysis were embedded in LR white resin, ultra-thin (100 nm) sections of it were sliced off using an Ultramicrotome mounted on a Carbon Cu grid. A field emission scanning electron microscope (FESEM), model UltraPlus FESEM from Carl Zeiss Inc., with an in-lens detector at 3kV and an aperture diameter of 30 µm, was also used to measure the coating thickness. In addition, an X-ray energy dispersive spectroscopy (X-EDS) FESEM tool was used to determine the chemical elements present in a specimen of both the ITO- and the SnO_2-coated fibre samples, on the cross-section portion of the metal coating. Further details are provided in Supporting Information.

Refractive index measurement.

For the characterization of both the ITO and the SnO_2 thin films, an ellipsometer UVISEL, with spectral range of 0.6–6.5 eV (190–2100 nm), an angle of incidence of 70°, a spot size of 1 mm, and Software DeltaPsi2TM (from Horiba Scientific Thin Film Division) were used.

Simulations.

For the unclad MMFs, after the deposition of the thin film and the Eudragit layer, the optical spectrum was calculated by means of a numerical analysis based on the well-known plane wave method for a one-dimensional multilayer waveguide,[25] validated for both SPRs[26] and LMRs.[21] The optical fibre cladding RI, made of fused silica, was estimated using the Sellmeier equation. FIMMWAVE® was used for the simulation in the D-shaped SMFs. The propagation was obtained with FIMMPROP, an integrated module of FIMMWAVE. Further details are provided in Supporting Information.

Results and Discussion

A biological sensing layer, selective to the target under investigation and deposited on the coated fibres, is essential for performing a bioassay. The biological sensing layer used in the present work consisted of antibodies as the biological recognition element, covalently anchored to the fibre surface, which exploit the functional groups of a deposited polymeric layer. The effect of the polymeric deposition onto the metal oxide-coated fibre samples was investigated. The λ_{LMR} of both ITO- and SnO_2-coated samples shifted in air towards longer wavelengths a total of (29 ± 1)

nm and (33 ± 1) nm, respectively, in repeated experiments, before and after the polymeric deposition. The shifts towards longer wavelengths can be explained by an increase in the overall coating thickness by the deposition of the polymeric layer, which agreed with the LMR theory.[21]

Afterwards, the nanocoatings deposited (i.e. ITO and SnO_2) were thoroughly analysed by means of TEM and SEM imaging, together with X-EDS tool, which led to the determination of the thickness of the deposited layer. The ITO thin film deposited on unclad MMFs was characterised by a thickness of (295 ± 5) nm, with the film thickness increasing up to (355 ± 5) nm, inferring that the thickness of the polymeric layer after the solvent evaporation was (60 ± 7) nm (Supporting Information, Figure S1). As for D-shaped SMF samples, the measured thickness of the deposited the SnO_2 thin film was (160 ± 5) nm, which increased to (220 ± 5) nm after the deposition of the polymeric layer, inferring that, also in this case, the thickness of the polymeric layer after the solvent evaporation was (60 ± 7) nm (Supporting Information, Figure S1).

The effects of the proposed thin-film deposition were also investigated from a theoretical point of view by considering the wavelength dependence of the refractive index RI (n) and extinction coefficient (k) of both ITO and SnO_2 nanometric films (Supporting Information, Figure S2). Moreover, the optical field intensity distribution of the fundamental mode (HE1,1) in the cross-section of both the ITO-coated unclad MMF and the SnO2-coated D-shaped SMF was also analysed (Supporting Information, Figure S3). The evanescent field generated at the film-surroundings interface was predictably larger in D-shaped SMFs, so expecting a great improvement in surface sensitivity.[27] As for the RI of the polymeric layer, the value used in the simulations was measured with an ellipsometer at two different wavelengths after evaporation of the solvent: 1.4921 (± 0.004) at 635 nm and 1.4568 (± 0.002) at 1550 nm. The numerical and experimental transmission spectra of ITO-coated unclad MMFs are presented in Figure 2a and 2b, respectively, as proof of concept on the effect of the thin film deposited on unclad MMFs, which generates the LMR. In accordance with the values obtained with SEM and TEM imaging (Supporting Information, Figure S1a-c), the ITO and Eudragit layers of 295 nm and 60 nm, respectively, were used for the simulation. The wavelength shift after deposition of the polymeric polymer can be explained thanks to the rules indicated in reference:[21] the LMR experienced a wavelength shift towards longer wavelengths if there is an increase in the thin film thickness, and the addition of the Eudragit increased the coating thickness. Moreover, the immersion of the sensor in water also led to an additional shift towards longer wavelengths, which agreed with the LMR theory.[17,21]

The same analysis was conducted for the thin-film deposited on the D-shaped SMF samples. In accordance with the values obtained with SEM and TEM imaging (Supporting Information, Figure S1e-f and S1h-i), the SnO_2 and Eudragit layers of 160 nm and 60 nm, respectively, were used for the simulation. Figure 2c and 2d show the theoretical and experimental results, respectively, when the fibre coated with SnO_2 and the Eudragit layers was immersed in water. Unlike the unclad MMFs, no optical spectrum obtained with D-shaped SMFs surrounded by air is presented because the LMR is so sensitive (it has optimal conditions: it is the first LMR, and it is located in the infrared region)[17,21] that the LMR shifts outside the spectral region monitored with the setup previously-described. As can be observed, the depth of the numerical resonance was slightly greater than that of the experimental one, because this parameter strongly depends on the distance between the deposited thin film and the fibre core, and thus on the polishing depth of the D-shaped SMFs provided by the manufacturer. In addition, in both cases, simulated λ_{LMR} exhibited a shift towards longer wavelengths as compared with experimental λ_{LMR}. However, the errors in λ_{LMR} (2.6% for the ITO-coated unclad MMF samples and 3.2% for the SnO_2-coated D-shaped SMF samples) were very small, and may have derived from an error in the measurement of the layer thickness.

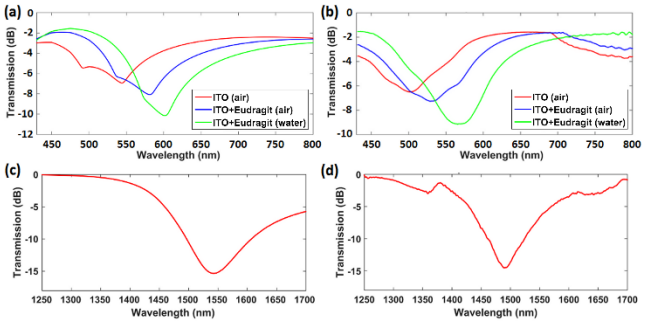

Figure 2. Numerical (a) and experimental (b) transmission spectra of ITO-coated unclad MMF samples evaluated in air and water before and after the polymeric (Eudragit L100) deposition. Numerical (c) and experimental (d) transmission spectra of SnO_2-coated D-shaped SMF samples evaluated in water after the polymeric deposition.

TEM and SEM imaging confirmed the predictions of the simulated results. The values of the thickness obtained were decisive in setting the LMR wavelength of the device. In fact, the spectral features of the LMR or any other kind of resonance, such as the transmission depth and bandwidth and the way employed of extracting the resonance minimum, could strongly influence the performance of the device, together with the experimental conditions during the bioassay implementation.[27]

The next step was the implementation of the IgG/anti-IgG assay and, hence, the real-time monitoring of the binding interactions during the bioassay for both the ITO- and SnO_2-coated LMR fibre sensors. After the preparation of the biological sensing layer (an example of real time monitoring of all those steps is shown in Supporting Information, Figure S4), increasing concentrations of the analyte spiked in serum were injected, by means of a peristaltic pump, within a flow cell containing the sensing device. Figure 3a details the sensorgram (signal change vs. time) of a SnO_2-coated unclad MMF biosensor, starting from the serum injection as the blank measurement followed by all the antigen concentrations from 1 μg L^{-1} up to 500 mg L^{-1}. All the values of λ_{LMR} in the sensorgram were calculated in

real time by means of the LMR tracking software (Supporting Information, Figure S5 and Figure S6). Figure 3b displays the sensor response to the serum injection and the subsequent rinsing with PBS. The shift of the λ_{LMR} taken in PBS before and after the serum injection, which contained various non-target species except for the specific analyte under investigation, was 0.04 nm averaged in repeated experiments, while the signal change of the first antigen concentration (1 μg L^{-1}) was 0.11 nm, i.e. 2.75-fold greater. This is the clear evidence of the high specificity of the sensing layer that did not interact with different biological species present in the serum. Since SnO_2-coated unclad MMF biosensors presented a higher sensitivity than the ITO coated unclad MMF biosensors, the next step was to analyse the SnO_2-coated D-shaped SMF biosensors. As above-mentioned, these devices were supposed to be more sensitive, given their geometrical structure, which made it possible to track the first LMR in the infrared region.[17] For this reason, lower concentrations of the analyte from 0.001 μg L^{-1} up to 1 μg L^{-1} were injected. The respective sensorgram is shown in Figure 3c. By considering the concentration in common between the two responses detailed in Figure 3a and Figure 3c (1 μg L^{-1}), the signal change taken in PBS after the antigen injection was (0.11 ± 0.03) nm for the SnO_2-coated unclad MMF biosensor and (1.89 ± 0.09) nm for the SnO_2-coated D-shaped SMF biosensor, i.e. 17-fold greater. Figure 3d displays the specificity test for this biosensor. The shift of the λ_{LMR} taken in PBS before and after the serum injection was 0.08 nm averaged in repeated experiments, while the signal change of the first antigen concentration (0.001 μg L^{-1}) was 0.3 nm, i.e. 3.75-fold greater. Even in this case, as for the SnO_2-coated unclad MMF biosensors, the high specificity of the sensing layer was confirmed.

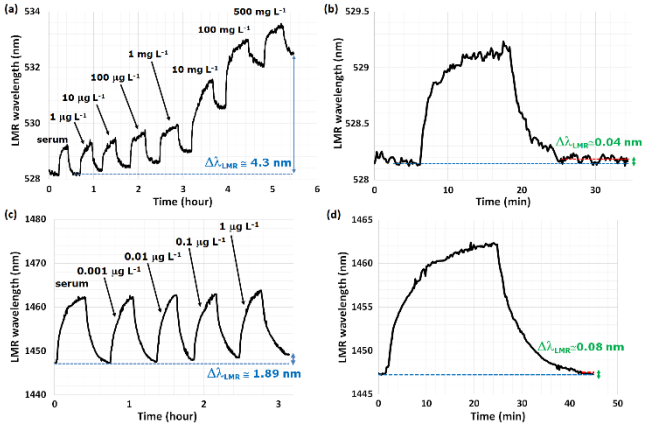

Figure 3. (a) Sensorgram of the SnO_2-coated unclad MMF biosensor starting from the serum, as the blank measurement, to all the antigen concentrations (1 μg L^{-1} – 500 mg L^{-1}) with a displayed total λ_{LMR} shift of roughly 4.3 nm (blue highlighted). (b) From the sensorgram, the signal change before and after the serum injection without the specific analyte (specificity test) is detailed with a total shift of roughly 0.04 nm. (c) Sensorgram of the SnO_2-coated D-shaped SMF biosensor starting from the serum to all the antigen concentrations (0.001–1 μg L^{-1}) with a displayed total λ_{LMR} shift of roughly 1.89 nm (blue highlighted). (d) Specificity test for the SnO_2-coated D-shaped SMF biosensor is detailed with a total shift of roughly 0.08 nm.

It is worth underlining that the LMR wavelengths reported on Figure 3 differ from those of Figure 2 since the sensors were placed inside the flow-cell, after the polymeric deposition carried out outside it. Moreover, by looking at Figure 3, it can be observed that the time to reach the steady-state slightly increased for the D-shaped SMF biosensor most likely due to the interaction of the flow with the sensor structure, which determined a different diffusion time of the biomolecules. Therefore, in order to maintain comparable times of measurement following the same bioassay protocol, the maximum LMR shift was not completely attained for the D-shaped SMF biosensor.

By drawing the shift of the λ_{LMR} as a function of the analyte concentration, it was possible to achieve the calibration curve of the biosensor (signal change vs. analyte concentration). As previously mentioned, a better performance of the D-shaped SMF sensors was expected. Two different sensors were used for a full characterization of the SnO_2-coated D-shaped SMF biosensor, sensor 1 and sensor 2, with sensor 1 focused on the higher concentration range (0.1 μg L^{-1} – 10 mg L^{-1}) and sensor 2 focused on the lower concentration range (0.001 – 1 μg L^{-1}). The sensorgram for sensor 2 is shown in Figure 3c. The measurements on the concentration range considered were repeated by regenerating the biological sensing layer with four full cycles for sensor 1 and three full cycles for sensor 2. Figure 4a shows the calibration curve that includes the measurements achieved with the two sensors (grey symbols for sensor 1 and black symbols for sensor 2), in which the results for each cycle are detailed together with the sigmoidal fit of the experimental points by using the Hill equation (green curve). The Hill equation, which is formally equivalent to the Langmuir isotherm, is a well-accepted mathematical model that provides a way in which to quantify the degree of interaction between ligand binding sites.[28] A correlation (R^2) coefficient of 0.9964 and a maximum deviation of the residuals of 0.2 nm were obtained from the data fitting. It is worth pointing out that the standard deviation of the experimental points was smaller than the size of the symbols (σ_{max} = 0.06 nm), with the standard deviation calculated by considering 15 subsequent acquisitions for each point under the same experimental conditions (flow stopped). Moreover, it is also important to point out the reproducibility, with the two different sensors obtaining the same values as those of the λ_{LMR} shift for the two concentrations in common (0.1 and 1 μg L^{-1}). The inset of Figure 4a details the experimental points obtained in the lower concentration range with the second cycle of sensor 2. The black error bars refer to the standard deviation of the experimental points. By comparing the results achieved at the concentrations in common between the two experiments, i.e. 0.1 μg L^{-1} and 1 μg L^{-1}, the standard deviation of the signals was 0.14 nm and 0.12 nm, respectively, i.e. comparable to the maximum deviation of the residuals obtained in the fitting procedure. By performing the same bioassay, Figure 4b shows a comparison of the calibration curves obtained with all three kinds of LMR sensors: ITO- (green triangles) and SnO_2-coated (red circles) unclad MMF biosensors, and

SnO_2-coated D-shaped SMF biosensor (sky blue rhombuses). Again, the value of the standard deviation of the experimental points in Figure 4b was smaller than the size of the symbols. By comparing the shifts of the λ_{LMR} obtained with the antigen concentration of 10 mg L^{-1}, the SnO_2-coated D-shaped SMF biosensor exhibited 6.4-fold and 3.6-fold shifts that were greater than those obtained with the ITO- and SnO_2-coated unclad MMF biosensors, respectively. Additional comparisons in surface sensitivity among the biosensors tested were discussed and provided in Supporting Information; for instance, the relative LMR wavelength shift (normalised by the LMR wavelength) is detailed in Figure S7.

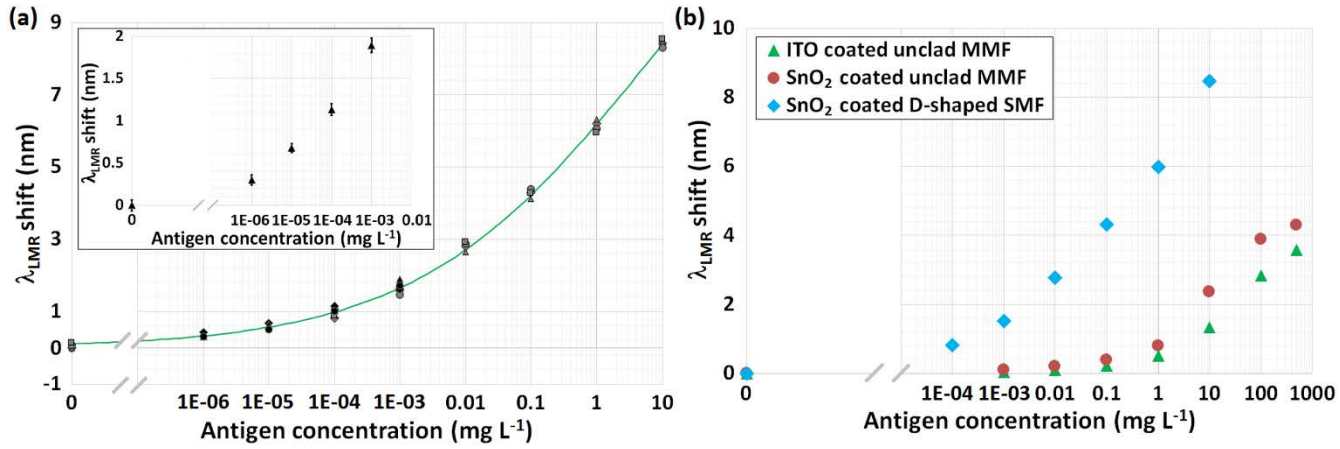

Figure 4. (a) Calibration curve of the SnO_2-coated D-shaped SMF biosensor repeated several times and displayed together with the sigmoidal fit of the experimental points (sensor 1: grey symbols; sensor 2: dark symbols). Each cycle of measurement corresponds to a different symbol. The antigen concentration is reported in log scale. The inset shows the enlargement of the calibration curve for the lower concentration range investigated with sensor 2 (second cycle), together with the respective standard deviation for each experimental point (black error bars). (b) Comparison of the calibration curves obtained with all three kinds of LMR sensors: the ITO- (green triangles) and SnO_2-coated (red circles) unclad MMF biosensors, and the SnO_2-coated D-shaped SMF biosensor (sky blue rhombuses).

By means of the calibration curve, it was possible to obtain the LOD of a biosensor. There are different approaches for evaluating the LOD.[27] If 3σ of the blank measurement (0.18 nm) is considered according to IUPAC recommendations, a LOD of 150 pg L^{-1} (1 fM) is attained. A different LOD of 0.6 ng L^{-1} (4 fM) is attained if 3σ of the maximum standard deviation obtained among all the experimental points (0.27 nm) is considered. All these values refer to the D-shaped SMF biosensors. By using this last approach, LODs of 3.5 μg L^{-1} and 0.9 μg L^{-1} were obtained from Figure 4b with the ITO- and SnO_2-coated unclad MMF biosensors, respectively.

After the implementation of the same bioassay in the same experimental conditions with both the ITO- and SnO_2-coated unclad MMF and D-shaped SMF biosensors, we compared the performance achieved in terms of LOD with other highest-performance fibre-based biosensors present in the literature. Table 1 collects all these results. Given the higher RI of tin dioxide as compared with the ITO, SnO_2-coated LMR samples, it was found to be capable of a better performance. Moreover, the same kind of sensor realised on the D-shaped SMFs achieved the best results in terms of LOD. The increase in sensitivity was apparent, and was expected, due to the larger evanescent field in the D-shaped nanocoated SMFs with respect to the standard unclad MMFs. On the other hand, biosensors based on long period gratings (LPGs)[24,29] reported a LOD of the order of μg L^{-1} (tens of pM) or slightly less. Considering different not-in-fibre systems for the detection of IgG, two examples reported on a LOD of the order of nM. In the former case, a smartphone platform based on SPR was developed (LOD of 47.4 nM) with the sensing element fabricated by a light-guiding silica capillary that was stripped off its cladding and coated with 50-nm gold film.[30] In the latter case, a label-free biosensor based on an engineered photonic crystal attained a LOD of 4.25 nM with the sensing element integrated into a smartphone platform.[31] Up-to-now, the literature has reported only one example of a biosensor based on an optical fibre device with a comparable LOD: a gold nanodisk array at the fibre end facet was used to measure free prostate-specific antigen.[32] In this case, the LOD claimed was obtained by performing the measurement in a simple buffer matrix, and not in a complex matrix such as serum, plasma or blood samples, thus expecting a higher LOD if the measurement was carried out on real complex samples. In addition, both the fabrication and preparation of the biosensor are quite long and complex, and involve the use of advanced, expensive and highly technical instrumentation. Therefore, except for this last case and when compared with other optical biosensing platforms used for the detection of proteins,[2,8,24,29-31] the LOD was enhanced by almost three orders of magnitude: a big leap in performance, undoubtedly! In addition, with this impressive step forward, the low level of the LOD achieved (a few fM in human serum) is perfectly comparable with, if not better than, the more well-established optical platforms based on SPR. For example, LODs of 200 fM and 350 fM have been claimed for the detection of miRNA in erythrocyte lysate[33] and for the carcinoembryonic antigen,[34] a cancer biomarker in plasma, respectively.

Table 1. Performance comparison in terms of LOD by using different fibre-based biosensors

Type of sensor	Target	Matrix	LOD	Reference
ITO-coated LMR unclad MMF	Immunoglobulin G	Serum	3.5 μg L^{-1} (23 pM)	present work
SnO_2-coated LMR unclad MMF	Immunoglobulin G	Serum	0.9 μg L^{-1} (6 pM)	present work
SnO_2-coated LMR D-shaped SMF	Immunoglobulin G	Serum	0.15 ng L^{-1} (1 fM)	present work
Titania-silica sol-gel coated LPG	Immunoglobulin G	Serum	8 μg L^{-1} (53 pM)	29
SPR-based silica capillary	Immunoglobulin G	PBS	7.1 mg L^{-1} (47.4 nM)	30
Engineered photonic crystal	Immunoglobulin G	Not specified	0.64 mg L^{-1} (4.25 nM)	31
Reflection-type coated LPG	Thyroglobulin	Not specified	Sub μg L^{-1} (< pM)	24
Gold nanodisk array localised SPR	Free prostate-specific antigen	PBS	0.1 ng L^{-1} (3 fM)	32

Another critical and crucial test involved the regeneration and reusability of the proposed optical fibre biosensors. The goal was achieved by using a solution of SDS. Figure 5 details all the steps of the regeneration test performed with an ITO-coated unclad MMF biosensor. The same experiment was repeated with a SnO_2-coated unclad MMF biosensor (Supporting Information, Figure S8 and Table S1). Here in Figure 5, the decrease in the signal after the SDS injection and PBS rinsing is a clear sign of the removal of the antigen by the regeneration solution from the antibody anchored on the sensor surface. The red-highlighted change in the signal details the first regeneration of the biosensing layer after the entire calibration procedure, in which 66% of the total dynamics was recovered. The green-highlighted plateaux represent the value of the blank signal, while the blue-highlighted ones represent the value of the signal after the injection of the analyte at 1 mg L^{-1}. This analyte concentration was selected since it was close to the IC50 inflection point of the calibration curve (i.e. the value of the analyte concentration for which the LMR wavelength shift equals to 50% of the dynamic signal range), as usually done in biosensing.[28] The regeneration procedure was repeated three times, showing the efficiency as well as the repeatability of the procedure. Since the regeneration does not depend on the sensor configuration but on the features of the biomolecules involved (i.e. affinity, electric charge, etc.), on the experimental conditions and on the regeneration protocol used, its effectiveness was proved with the unclad MMF devices.

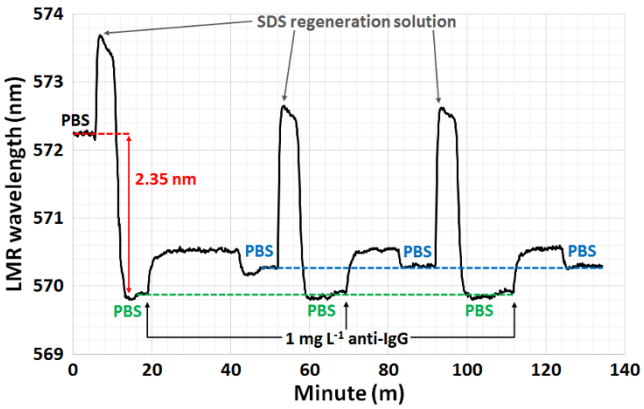

Figure 5. Regeneration test with the SDS solution repeated three times by using the ITO-coated unclad MMF biosensors (analyte concentration of 1 mg L^{-1}). The red-highlighted change of the signal shows the first regeneration of the biosensing layer after the entire calibration procedure. The green-highlighted plateaux represent the value of the blank signal, while the blue-highlighted ones represent the value of the signal after the analyte injection.

Conclusions

Two different optically absorbing materials, i.e. indium tin oxide and tin dioxide, were deposited on multimode and D-shaped fibres in order to excite lossy mode resonances, which are recently-explored physical phenomena for the development of label-free biosensors different from the well-known surface plasmon resonance but able to attain high sensitivity and resolution in any case. The nm-thick depositions were numerically and experimentally analysed showing a good agreement. Thanks to TEM and SEM imaging, it was possible to set the resonances in the preferred wavelength range and to obtain a reliable thickness of the polymeric layer deposited on the fibres in order to functionalise their surface. We encompassed all the most important steps in an analytical methodology for sensing purposes: design and fabrication, modification, integration, application to a bio-interaction analysis and regeneration. In fact, considering that the proposed nano-coated optical fibre biosensors, with the best performance obtained by using SnO_2-coated D-shaped single-mode fibres, were integrated into a thermo-stabilized flow-cell, it enabled us to address all the typical requirements that a real biosensor must possess with a view to the development of an *in situ*, portable, lightweight and high-performance optical platform for biochemical and biomedical applications.

Two critical but very important issues with regard to all biosensors were also addressed by using SnO_2-coated D-shaped SMF biosensors. First, not only the repeatability but also the reproducibility of the results were experimentally proved on fibre-based biosensors, with the results obtained with two different sensors lying perfectly on the same calibration curve (Figure 4a). Second, given the defi-

nition of LOD and the way it is calculated, it is almost impossible to find even one experimental point below or very close to the LOD claimed in the literature up until now.

The ability of the proposed biosensors to attain ultra-low LOD, combined with a capability to be integrated within a reliable optical platform, reveals in a tangible way the potential of fibre-based sensors to play a fundamental role in the biomedical field, where the demand on the part of physicians for devices capable of identifying the onset of diseases at a very early stage or of performing measurements in real time close to the patient's bed is continuously on the increase.[35]

ASSOCIATED CONTENT

Supporting Information. Details of TEM and SEM imaging, of the approach used for simulations, of the bioassay protocol used, of the software tools for LMR tracking, of the additional comparisons in surface sensitivity and of the regeneration experiments performed. Supporting figures, references and a table hold up the manuscript. This material is available free of charge via the Internet at http://pubs.acs.org.

AUTHOR INFORMATION

Corresponding Authors

* Francesco Chiavaioli, "Nello Carrara" Institute of Applied Physics, National Research Council of Italy, Via Madonna del Piano 10, 50019 Sesto Fiorentino, Firenze, Italy, Tel.+39-055-522-6318, f.chiavaioli@ifac.cnr.it.
* Ignacio Del Villar, Institute of Smart Cities, Public University of Navarra, Jeronimo de Ayanz Center, Campus Arrosadia, 31006 Pamplona, Spain; Tel. +34-94-816-9256, ignacio.delvillar@unavarra.es.

Author Contributions

F.C., I.D.V., F.J.A., I.R.M. and F.B. conceived the project. P.Z. and C.R.Z. conceived the sensors. F.C., P.Z. and C.R.Z. characterized properties of sensors. F.C., P.Z. and C.T. designed and performed the experiments, and analysed the data. C.T. developed the software tools for tracking the resonances. A.G. and S.T. prepared all the chemicals. I.D.V. conceived the theoretical analysis and performed the simulations. F.J.A., I.R.M. and F.B. supervised the project. F.C., I.D.V. and A.G. wrote the manuscript. All authors have given approval to the final version of the manuscript. ‡These authors contributed equally.

ACKNOWLEDGMENT

This work was supported by the European Community for the project Hemospec (FP7-611682), by the Italian National Research Council for the Short Term Mobility program 2017 and by the Spanish Agencia Estatal de Investigación (AEI) and European Regional Development Fund (FEDER) (TEC2016-78047-R, TEC2016-79367-C2-2-R).

REFERENCES

(1) Rajan, G. *Optical fiber sensors: advanced techniques and applications*; CRC Press, Taylor & Francis Group, 2015.
(2) Chiavaioli, F.; Baldini, F.; Tombelli, S.; Trono, C.; Giannetti, A. Biosensing with optical fiber gratings. *Nanophotonics* **2017**, 6, 663–679.
(3) Caucheteur, C.; Guo, T.; Liu, F.; Guan, B.O.; Albert, J. Ultrasensitive plasmonic sensing in air using optical fibre spectral combs. *Nat. Commun.* **2016**, 7, 13371.
(4) Stern, L.; Desiatov, B.; Mazurski, N.; Levy, U. Strong coupling and high-contrast all-optical modulation in atomic cladding waveguides. *Nat. Commun.* **2017**, 8, 14461.
(5) Ye, X.W.; Su, Y.H.; Han, J.P. Structural health monitoring of civil infrastructure using optical fiber sensing technology: a comprehensive review. *Sci. World J.* **2014**, 2014, article ID 652329.
(6) Lefevre, H.C. *The fibre-optic gyroscope*, 2nd ed.; Artech House, 2014.
(7) Wang, X.D.; Wolfbeis, O.S. Fiber-optic chemical sensors and biosensors (2013-2015). *Anal. Chem.* **2016**, 88, 203–227.
(8) Vaiano, P.; Carotenuto, B.; Pisco, M.; Ricciardi, A.; Quero, G.; Consales, M.; Crescitelli, A.; Esposito, E.; Cusano, A. Lab on fiber technology for biological sensing applications. *Laser Photonics Rev.* **2016**, 10, 922–961.
(9) Devi, R.V.; Doble, M.; Verma, R.S. Nanomaterials for early detection of cancer biomarker with special emphasis on gold nanoparticles in immunoassays/sensors. *Biosens. Bioelectron.* **2015**, 68, 688–698.
(10) Wang, R.; Zhou, X.; Zhu, X.; Yang, C.; Liu, L.; Shi, H. Isoelectric bovine serum albumin: robust blocking agent for enhanced performance in optical-fiber based DNA sensing. *ACS Sens.* **2017**, 2, 257–262.
(11) Gramotnev, D.K.; Bozhevolnyi, S.I. Plasmonics beyond the diffraction limit. *Nat. Photonics* **2010**, 4, 83–91.
(12) Kretschmann, H.; Raether, E. Radiative decay of non radiative surface plasmons excited by light. *Zeitschrift für Naturforschung A* **1968**, 23, 2135–2136.
(13) Yang, F.; Sambles, J.R. Determination of the optical permittivity and thickness of absorbing films using long range modes. *J. Mod. Opt.* **1997**, 44, 1155–1164.
(14) Andreev, A.; Pantchev, B.; Danesh, P.; Zafirova, B.; Karakoleva, E.; Vlaikova, E.; Alipieva, E. A refractometric sensor using index-sensitive mode resonance between single-mode fiber and thin film amorphous silicon waveguide. *Sens. Actuators, B* **2005**, 106, 484–488.
(15) Tiwari, D.; Mullaney, K.; Korposh, S.; James, S.W.; Lee, S-W.; Tatam, R.P. An ammonia sensor based on lossy mode resonances on a tapered optical fibre coated with porphyrin-incorporated titanium dioxide. *Sens. Actuators, B* **2017**, 242, 645–652.
(16) Batchman, T.E.; McWright, G.M. Mode coupling between dielectric and semiconductor planar waveguides. *IEEE J. Quantum Electron.* **1982**, QE-18, 782–788.
(17) Del Villar, I.; Arregui, F.J.; Zamarreño, C.R.; Corres, J.M.; Bariain, C.; Goicoechea, J.; Elosua, C.; Hernaez, M.; Rivero, P.J.; Socorro, A.B.; Urrutia, A.; Sanchez, P.; Zubiate, P.; Lopez, D.; De Acha, N.; Ascorbe, J.; Matias, J.R. Optical sensors based on lossy-mode resonances. *Sens. Actuators, B* **2017**, 240, 174–185.
(18) Usha, S.P.; Mishra, S.K.; Gupta B.D. Fiber optic hydrogen sulfide gas sensors utilizing ZnO thin film/ZnO nanoparticles: a comparison of surface plasmon resonance and lossy mode resonance. *Sens. Actuators, B* **2015**, 218, 196–204.
(19) Zamarreño, C.R.; Hernáez, M.; Del Villar, I.; Matías, I.R.; Arregui, F.J. Optical fiber pH sensor based on lossy-mode resonances by means of thin polymeric coatings. *Sens. Actuators, B* **2011**, 155, 290–297.

(20) Homola, J. Surface plasmon resonance sensors for detection of chemical and biological species. *Chem. Rev.* **2008**, 108, 462–493.
(21) Del Villar, I.; Hernaez, M.; Zamarreño, C.R.; Sánchez, P.; Fernández-Valdivielso, C.; Arregui, F.J.; Matías, I.R. Design rules for lossy mode resonance based sensors. *Appl. Opt.* **2012**, 51, 4298–4307.
(22) Shalabney, A.; Abdulhalim, I. Figure-of-merit enhancement of surface plasmon resonance sensors in the spectral interrogation. *Opt. Lett.* **2012**, 37, 1175–1177.
(23) Andreev, A.T.; Zafirova, B.S.; Karakoleva, E.I.; Dikovska, A.O.; Atanasov, P.A. Highly sensitive refractometers based on a side-polished single-mode fibre coupled with a metal oxide thin-film planar waveguide. *J. Opt. A: Pure Appl. Opt.* **2008**, 10, 35303.
(24) Quero, G.; Consales, M.; Severino, R.; Vaiano, P.; Borriello, A.; Diodato, L.; Zuppolini, S.; Giordano, M.; Nettore, I.C.; Mazzarella, C.; Colao, A.; Macchia, P.E.; Santorelli, F.; Cutolo, A.; Cusano, A. Long period fiber grating nano-optrode for cancer biomarker detection. *Biosens. Bioelectron.* **2016**, 80, 590–600.
(25) Ota, R.; Seki, S.; Ogawa, M.; Nishide, T.; Shida, A.; Ide, M.; Sawada, Y. Fabrication of indium–tin-oxide films by dip coating process using ethanol solution of chlorides and surfactants. *Thin Solid Films* **2002**, 411, 42–45.
(26) Sharma, A.K.; Gupta, B.D. On the sensitivity and signal to noise ratio of a step-index fiber optic surface plasmon resonance sensor with bimetallic layers. *Opt. Commun.* **2005**, 245, 159–169.
(27) Chiavaioli, F.; Gouveia, C.A.J.; Jorge, P.A.S.; Baldini, F. Towards a uniform metrological assessment of grating-based optical fiber sensors: from refractometers to biosensors. *Biosensors* **2017**, 7, 32.
(28) Gesztelyi, R.; Zsuga, J.; Kemeny-Beke, A.; Varga, B.; Juhasz, B.; Tosaki, A. The Hill equation and the origin of quantitative pharmacology. *Archive for History of Exact Sciences* **2012**, 66, 427–438.
(29) Chiavaioli, F.; Biswas, P.; Trono, C.; Jana, S.; Bandyopadhyay, S.; Basumallick, N.; Giannetti, A.; Tombelli, S.; Bera, S.; Mallick, A.; Baldini, F. Sol–gel-based titania–silica thin film overlay for long period fiber grating-based biosensors. *Anal. Chem.* **2015**, 87, 12024–12031.
(30) Liu, Y.; Liu, Q.; Chen, S.; Cheng, F.; Wang, H.; Peng, W. Surface plasmon resonance biosensor based on smart phone platforms. *Sci. Rep.* **2015,** 5, 12864.
(31) Gallegos, D.; Long, K.D.; Yu, H.; Clark, P.P.; Lin, Y.; George, S.; Natha, P.; Cunningham, B.T. Label-free biodetection using a smartphone. *Lab Chip* **2013,** 13, 2124-2132.
(32) Sanders, M.; Lin, Y.; Wei, J.; Bono, T.; Lindquist, R.G. An enhanced LSPR fiber-optic nanoprobe for ultrasensitive detection of protein biomarkers. *Biosens. Bioelectron.* **2014**, 61, 95–101.
(33) Vaisocherová, H.; Šípová, H.; Víšová, I.; Bocková, M.; Špringer, T.; Ermini, M.L.; Song, X.; Krejčík, Z.; Chrastinová, L.; Pastva, O.; Pimková, K.; Dostálová Merkerová, M.; Dyr, J.E.; Homola, J. Rapid and sensitive detection of multiple microRNAs in cell lysate by low-fouling surface plasmon resonance biosensor. *Biosens. Bioelectron.* **2015**, 70, 226–231.
(34) Špringer, T.; Homola, J. Biofunctionalized gold nanoparticles for SPR-biosensor-based detection of CEA in blood plasma. *Anal. Bioanal. Chem.* **2012**, 404, 2869–2875.
(35) Luppa, P.B.; Bietenbeck, A.; Beaudoin, C.; Giannetti, A. Clinically relevant analytical techniques, organizational concepts for application and future perspectives of point-of-care testing. *Biotechnol. Adv.* **2016**, 34, 139–160.

The deposition of nm-thick tin dioxide films on specialty optical fibres, such as D-shaped fibres, generates lossy mode resonances with enhanced light-matter interaction that makes it possible to measure precisely and accurately the changes in optical properties of the fibre-surrounding medium with very high sensitivity. The biosensor proposed permits to detect analyte concentrations down to femtomolar in human serum.